



HAL
open science

Matter wave scattering on an amplitude-modulated optical lattice

Pierrick Cheiney, Charlotte Fabre, François Vermersch, Giovanni Luca Gattobigio, Renaud Mathevet, Thierry Lahaye, David Guéry-Odelin

► **To cite this version:**

Pierrick Cheiney, Charlotte Fabre, François Vermersch, Giovanni Luca Gattobigio, Renaud Mathevet, et al.. Matter wave scattering on an amplitude-modulated optical lattice. 2012. hal-00708994v1

HAL Id: hal-00708994

<https://hal.science/hal-00708994v1>

Preprint submitted on 16 Jun 2012 (v1), last revised 11 Jan 2013 (v2)

HAL is a multi-disciplinary open access archive for the deposit and dissemination of scientific research documents, whether they are published or not. The documents may come from teaching and research institutions in France or abroad, or from public or private research centers.

L'archive ouverte pluridisciplinaire **HAL**, est destinée au dépôt et à la diffusion de documents scientifiques de niveau recherche, publiés ou non, émanant des établissements d'enseignement et de recherche français ou étrangers, des laboratoires publics ou privés.

Matter wave scattering on an amplitude-modulated optical lattice

P. Cheiney, C. M. Fabre, F. Vermersch, G. L. Gattobigio, R. Mathevet, T. Lahaye and D. Guéry-Odelin^{1,2}

¹Université de Toulouse, UPS, Laboratoire Collisions Agrégats Réactivité, IRSAMC; F-31062 Toulouse, France

²CNRS, UMR 5589, F-31062 Toulouse, France

(Dated: June 16, 2012)

We experimentally study the scattering of guided matter waves on an amplitude-modulated optical lattice. We observe different types of frequency-dependent dips in the asymptotic output density distribution. Their positions are compared quantitatively with numerical simulations. A semiclassical model that combines *local* Floquet-Bloch bands analysis and Landau-Zener transitions provides a simple picture of the observed phenomena in terms of elementary *Floquet photon* absorption-emission processes and envelope induced reflections. Finally, we propose and demonstrate the use of this technique with a bichromatic modulation to design a tunable sub-recoil velocity filter.

PACS numbers: 03.75.Kk, 03.75.Lm

Cold atoms interacting with time-modulated optical lattice display a wide variety of quantum and classical dynamics. These include the observations of dynamical localization [1, 2], chaos-assisted tunneling [3, 4], the Anderson metal-insulator transition in momentum space [5], dynamically controlled tunneling [6–8], or the probing of gapped modes in degenerate quantum gases [9, 10].

In this Letter we propose and demonstrate the use of time-dependent optical lattice for atom optics. We investigate the scattering of a cold atom packet on an amplitude-modulated optical lattice [11–14]. Our technique provides a new tunable tool for velocity selection in confined geometries and a system for studying quantum transport with time-dependent potentials [15] as initially studied in mesoscopic physics [16, 17].

The Bragg reflection of a propagating guided matter wave on a static optical lattice has been recently demonstrated [18]. The Bragg condition on the class of velocities that are reflected reads $v_{\text{Bragg}} = nv_L/2$ where n is an integer, $v_L = h/(md)$ and d is the lattice spacing. This condition is valid in the perturbative limit i.e. for a small-depth optical lattice $U_0 \ll E_L$ where $E_L \equiv mv_L^2/2$ is the lattice energy scale. However v_{Bragg} is directly related to the periodicity of the lattice and therefore cannot be easily tuned over a large range.

In contrast, the interaction of a propagating matter wave with an amplitude-modulated optical lattice gives rise to a wide variety of phenomena, and realizes, in particular, a tunable Bragg reflector. Our study explores the non perturbative regime for which the lattice depth is not small compared to the lattice energy scale E_L and the modulation depth is relatively large. We will show how the observed phenomena on the different class of velocity can be understood in terms of simple pictures using a semiclassical model that combines the local Floquet-Bloch framework and Landau-Zener transitions. We finally take advantage of our understanding to demonstrate experimentally the interest of such a system to engineer the momentum distribution of a propagating wave packet.

Our experimental setup has already been described in [18]. In short, a thermal cloud of typically 8.10^4

rubidium-87 atoms at $T = 500$ nK is obtained after 3.5 s of forced evaporation in a crossed dipole trap formed by two red-detuned (1070 nm) laser beams: a horizontal guide and a dimple beam. During the evaporation, we use the spin-distillation technique to prepare atoms in $|F = 1, m_F = 0\rangle$ [19, 20]. We deliberately use a thermal cloud rather than a BEC in order to probe the modulated lattice for a wide range of velocities in a single shot (see below). By switching off the dimple beam, we release a packet of longitudinal velocity dispersion $\Delta v = 6$ mm/s in the horizontal guide. Atoms are subsequently accelerated by a $t_{\text{acc}} = 15$ ms inhomogeneous magnetic field pulse to a mean velocity $\bar{v} = 10$ mm/s. The atomic packet then propagates towards the lattice whose center is located $500 \mu\text{m}$ downstream from the trap position (see Fig. 1(a)). The lattice is obtained by crossing two horizontal off-resonance laser beams (wavelength $\lambda = 840$ nm, waist $w = 100 \mu\text{m}$) at an angle $\theta = 81^\circ$ [18]. We modulate the lattice intensity using an acousto-optic modulator prior to the beam separation. The time-dependent potential experienced by the atoms reads:

$$U(x, t) = -U_0(t)e^{-2x^2/\tilde{w}^2} \sin^2\left(\frac{\pi x}{d}\right), \quad (1)$$

where $U_0(t) = U_0(1 + \eta \cos(2\pi\nu t))$, $d = \lambda/[2 \sin(\theta/2)] = 650 \pm 15$ nm ($v_L = 7.1$ mm/s, $E_L/h = \nu_L = 5.4$ kHz) and $\tilde{w} = w/\cos(\theta/2) \simeq 130 \mu\text{m}$. The lattice depth $U_0 = 2E_L$ is calibrated by Kapitza-Dirac diffraction [21]. The typical modulation depth is $\eta = 33\%$. The atomic packet propagates during $t_{\text{prop}} = 78$ ms, through the lattice and is imaged *in-situ* (with no time-of-flight) by absorption imaging.

Figure 1(b) shows the atomic density after propagation as a function of the modulation frequency ν . Each line is obtained by averaging 8 images integrated along the transverse direction. Figure 1(c) is the result of a numerical simulation of the atomic packet dynamics using the one-dimensional Schrödinger equation solved by the split-Fourier method and a wave packet whose initial momentum and position dispersions match the measured experimental values. Atom-atom interactions are negli-

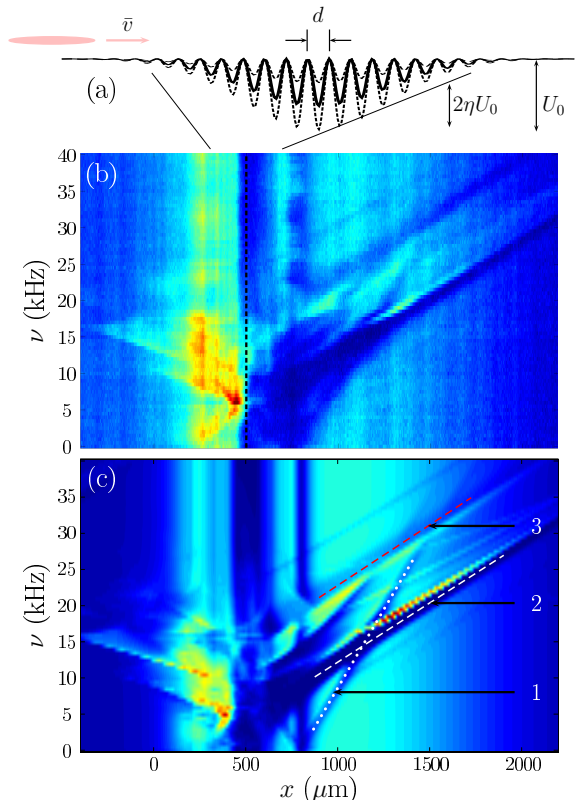


FIG. 1: (color online) (a) Sketch of a propagating atomic packet impinging onto an optical lattice whose amplitude is modulated. (b) Measured longitudinal density $n(x, t_{\text{acc}} + t_{\text{prop}})$ after an acceleration stage of $t_{\text{acc}} = 15$ ms and a propagation time $t_{\text{prop}} = 78$ ms for various lattice modulation frequencies ν (lattice depth $U_0 = 2E_L$, modulation depth $\eta = 33\%$, lattice position given by the dotted line). (c) Numerical simulations (see text) with a resolution that matches the experimental optical resolution ($\sim 10 \mu\text{m}$). Frequency-dependent dips are observed in the transmitted distribution. Dotted and dashed lines in (c) show the linear dependence of the dip position with ν .

gible in the course of the propagation. We find a good agreement between simulations and experiment.

Except for the zones very close to depletion lines in the transmitted part in Fig. 1(b), each position downward the lattice can be mapped onto a well defined class of incident velocity $x \simeq v_{\text{inc}}(t_{\text{acc}} + t_{\text{prop}}) + K$ where K is a constant [22]. Two kinds of density dips are observed in the transmitted part: (i) dips whose positions do not depend on the modulation frequency and that correspond to velocity classes fulfilling the Bragg reflection on the *static* lattice [18], and (ii) dips whose positions depend on the frequency. As we shall discuss below, some dips of the latter category have their counterpart in the reflected packet and correspond to reflected class of velocity while others are due to slowing down or acceleration effects. Using the correspondence between x and v_{inc} , the white dashed line in Fig. 1(c) has a slope $(660 \text{ nm})^{-1} \simeq 1/d$

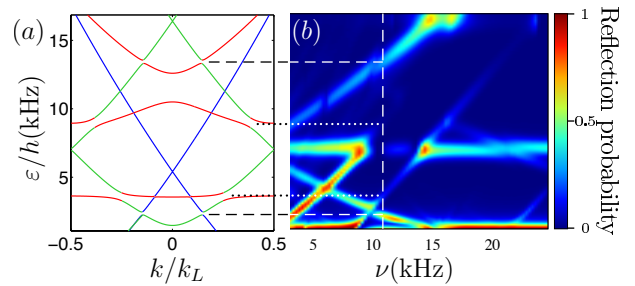


FIG. 2: (color online) (a) Floquet-Bloch band diagram for a square-envelope lattice (depth $U_0 = 2E_L$) and modulation frequency $\nu = 11$ kHz. Band color code: green $-0.5 < \langle n_F \rangle < 0.5$, red $\langle n_F \rangle > 0.5$ and blue $\langle n_F \rangle < -0.5$ where n_F is the Floquet excitation number. (b) Probability of reflection obtained from a numerical simulation of a 1D wavepacket with an incident velocity dispersion $\Delta v = 0.2$ mm/s impinging on time amplitude-modulated lattice with a finite square-envelope (length= $80 d$, $U_0 = 2E_L$, $\eta = 30\%$) as a function of the incident energy and ν . The horizontal white dashed line shows the case $\nu = 11$ kHz that corresponds to the diagram (a). The horizontal dashed (dotted) lines denotes open gap (degenerate) anticrossings. Only open gap anticrossings yield reflection.

and we observe the corresponding reflected atoms in the region $x < 0$. The red upper dashed line of depleted atoms in Fig. 1(c) is parallel to the main line and has no counterpart in the reflected region. The white dotted line in Fig. 1(c) has a slope three times as large as those of the white and red depletion lines in Fig. 1(c). The slopes and their relative position can be simply interpreted in terms of interband transitions in the limit of a small lattice depth. Indeed, in this case, the band structure can be nearly exactly constructed by the superposition of parabolic energy spectra centered around all reciprocal points $E_n(k) = \hbar^2(k - nk_L)^2/2m$, where n is an integer and $k_L = 2\pi/d$. The one *Floquet photon* transition frequencies are given by [23]

$$\pm\nu_{n \rightarrow n'} = \frac{E_n - E_{n'}}{h} = -(n - n')^2\nu_L + \frac{n' - n}{d}v_0,$$

where v_0 is the incident velocity. The different transition lines (depending on the incident velocity) associated with the observed depletion lines can be identified. In this way, we find a slope of $3/d$ for the white dotted line and a slope of $1/d$ for the dashed lines. The offset between the red and white dashed lines is $2\nu_L \simeq 10.8$ kHz. These predictions are in good agreements with our data. To get a better understanding of the width of the depletion lines, their interpretation in terms of elementary processes, the timescale on which the transitions occur and the role played by the Gaussian envelope of the lattice potential, we introduce now a more elaborated analysis based on Floquet-Bloch framework [24, 25].

This approach is not restricted to small modulation depth and is thus well-adapted to analyze the experimental situation. For a potential periodic in both space and

time, the Floquet-Bloch solutions of the time-dependent Schrödinger equation read:

$$\psi_{n,k}(x,t) = e^{i(kx - \varepsilon_n(k)t/\hbar)} u_{n,k}(x,t), \quad (2)$$

where $\varepsilon_n(k)$ are the quasi-energies. The functions $u_{n,k}(x,t)$ are biperiodic in space and time and therefore can be Fourier expanded:

$$u_{n,k}(x,t) = u_{n,k}(x+d,t) = u_{n,k}(x,t+T) \\ = \sum_p \sum_{n_F} \phi_{n,k}^{n_F,p} e^{i(pk_L x - n_F \omega t)}. \quad (3)$$

In the following, we restrict ourselves to $n_F \in \{-1, 0, 1\}$ i.e. to situations in which only one *Floquet photon* can be absorbed or emitted [26]. At zero modulation depth, the Floquet-Bloch band diagram is nothing but the superposition of the Bloch diagrams shifted by $n_F \hbar \omega$. At finite modulation depth, anticrossings appear for frequencies that correspond to interband transitions.

Consider first the simple case of a square-envelope lattice of amplitude U_0 modulated at a frequency ν with an amplitude η . In Fig. 2(a) we plot the Floquet-Bloch spectrum for $\nu = 11$ kHz. Two kinds of anticrossings can be identified: those yielding open gaps (horizontal dashed line in Fig. 2) and those without gaps for which two states with the same quasi-energy are available (horizontal dotted line in Fig. 2). To identify the role of the different types of anticrossings on the incident matter wave packet, we have performed a 1D simulation which solves the corresponding time-dependent Schrödinger equation. Figure 2(b) gives the reflection coefficient as a function of the incident energy E_0 and the modulation frequency ν . Two types of reflection conditions can be clearly identified: (i) those due to Bragg reflection onto the static lattice (no dependence on ν) and (ii) those that correspond to open gap anticrossings and whose position depend on ν . The interpretation is clear when the incident energy falls in an open gap anticrossing, no propagating state is available and the particle is reflected [27]. The degenerate anticrossings do not induce reflection in the square-envelope case. However, as we discuss below, they play an important role in the dynamics of the experimentally relevant case in which the lattice has a slowly varying envelope.

In this latter case, the situation turns out to be radically different since the system can follow adiabatically a quasi-energy band during its time evolution. To describe this propagation, we propose a semiclassical model that enables one to identify the elementary processes responsible for the velocity changes of the particle and the time at which such processes occur. It contains two main ingredients. The first one consists in describing the particle motion on a given *local* Floquet-Bloch band through the combined evolution of the wavepacket position and of its mean pseudo momentum k . The corresponding set of coupled equations reads

$$\dot{x} = \frac{1}{\hbar} \frac{\partial \varepsilon_n}{\partial k} \quad \text{and} \quad \dot{k} = -\frac{1}{\hbar} \frac{\partial \varepsilon_n}{\partial x}. \quad (4)$$

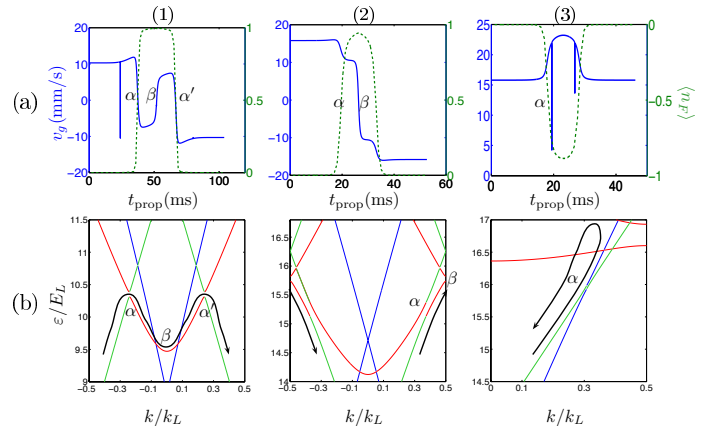


FIG. 3: (color online) (a) Velocity and mean Floquet excitation number $\langle n_F \rangle$ as a function of the propagating time for parameters corresponding to three different depletion zones shown in Fig. 1. (b) Local Floquet-Bloch diagram. Dark arrow denotes the trajectory followed by the fictitious particle of the semiclassical model (see text). Case (1): Reflection on an open gap $v = 10.3$ mm/s, $\nu = 11$ kHz. Case (2): Reflection on an anticrossing without gap $v = 15.8$ mm/s, $\nu = 20$ kHz. Case (3) transient acceleration $v = 15.8$ mm/s, $\nu = 30.5$ kHz. α (β) denotes absorption or emission of one *Floquet photon* (reflection).

The first equation defines the group velocity of the wave packets while the second results from the adiabatic following condition $d\varepsilon_n(k,x)/dt = 0$ [24, 28]. The second ingredient consists in taking into account the possibility for a particle to undergo a Landau-Zener transition when it passes an anticrossing. In our case, the approximation of a local two-level situation is valid and therefore the probability to change the band index is $P = e^{-2\pi\gamma}$ with

$$\gamma = \frac{\Delta E^2}{4\hbar} \left| \frac{d}{dt} (\varepsilon_n - \varepsilon_{n\pm 1}) \right|^{-1} \quad (5)$$

where ΔE is the size of the gap [29, 30]. In our simulated semiclassical trajectories, the band index is changed when $P > 0.5$ [31]. In this picture, the dynamics appears as an evolution that combines motions on a given band and sudden changes of band index.

Within this model, we can analyze the different mechanisms yielding to depletion bands as observed in Fig. 1. To illustrate the wide variety of possibilities, we shall choose three generic and different set of parameters (v_i, ν) yielding to dips in the output density distribution (see labels 1, 2 and 3 in Fig. 1(c)). In Fig. 3(a), we plot the velocity along with the mean Floquet excitation number for each case. In Fig. 3(b) we show the corresponding Floquet-Bloch diagrams in the region of interest. When a particle is moving toward the center, all quasi energies decrease since the amplitude of the attractive lattice increases. As a result, the particle state moves up relatively to the band diagram. In the same way, if the particle is moving backward, it will go down the hills of

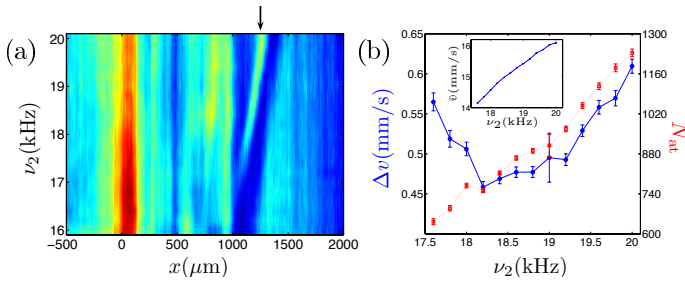


FIG. 4: (color online) (a) Density distribution for the scattering on a two-frequency modulated optical lattice (same conditions as in Fig. 1) for a fixed frequency $\nu_1 = 16$ kHz and a scanned frequency ν_2 . A narrow slice of transmitted atoms is produced (see arrow). (b) Number of atoms and velocity dispersion associated with these narrow slices of transmitted atoms as a function of ν_2 . Inset: mean velocity of the slice of atoms as a function of ν_2 .

the diagram. With these simple pictures in mind trajectories can be readily interpreted. In each case, the key phenomenon is the absorption or stimulated emission of a *Floquet photon* by adiabatic following denoted by α in Fig. 3. In case (1), the particle emits a *Floquet photon*, performs a reflection (denoted β) when reaching the bottom of the band and absorbs a *Floquet photon* (α') before leaving the lattice. In case (2), the first emission only slows down the particle which is then Bragg reflected and subsequently accelerated by *Floquet photon* absorption. In case (3), the particle is not reflected. It is transiently accelerated in the lattice by a *Floquet photon* absorption-emission cycle.

Other features of the experimental and numerical diagrams of Fig. 1 can be readily explained thanks to our semiclassical model. For instance, the density bump above the white dashed line that corresponds to atoms that have been slowed down. The velocity spread of reflected particles at position 2 (see Fig. 1) is 0.8 mm/s. This value can be recovered from the variation of the energy position of the gap along the lattice.

For a given incident kinetic energy E_0 , a large size of the envelope and/or a large modulation depth increases the efficiency of the process since it favors an adiabatic following of the anticrossings. A less intuitive feature concerns the lattice depth. Indeed, a small lattice depth ($U_0 < E_0$) increases the selectivity of the class of incident velocities that are affected by the modulation. This originates from the fact that the system is projected on a high energy band, and the position of the gap remains roughly

constant throughout the lattice. Interestingly enough, this ensures the robustness of the method against the specific shape of a smooth envelope.

We finally demonstrate that our device can be used as a tunable momentum filter by combining different modulation frequencies. We rely here on the main reflection line (white dashed line in Fig. 1) that acts as a notch filter in momentum space. We shall now modulate the lattice with two different frequencies to create a transmitted band between two rejected ones: $U_0(t) = U_0(1 + \eta \cos(2\pi\nu_1 t) + \eta \cos(2\pi\nu_2 t))$. Strictly speaking, the detailed dynamics of a wave packet submitted to this two frequency and non perturbative modulation cannot be inferred directly from the single frequency dynamics [32]. However, the simple picture according to which nearly independent “dips” can be drilled into the velocity distribution with two frequencies is quite robust. We observe that the reflection spectrum is roughly the product of the two independent spectra (see Fig. 4) [33]. The mean velocity of the slice of atoms is therefore governed by $d(\nu_1 + \nu_2)/2$ while its width is controlled by the frequency difference $|\nu_2 - \nu_1|$. In our set of experiments, ν_1 is fixed at 16 kHz and ν_2 is varied from 16 to 20 kHz. Between the two reflection lines, atoms in a narrow class of velocity are transmitted (arrow in Fig. 4). The slice contains about 1000 atoms and has a mean velocity on the order of 15 mm/s (inset of Fig. 4). The minimum velocity dispersion of the velocity filter that we have designed is on the order of 450 $\mu\text{m/s}$ for our parameters (i.e. 1.1 nK in temperature units).

In contrast with other techniques to select or manipulate the velocity distribution such as Doppler sensitive stimulated Raman transitions and coherent population trapping into a dark state (see [34] and references therein), our technique does not rely on specific internal level configuration and is adapted to guided atom optics. A further improvement of velocity selection could be achieved using a smaller depth lattice combined with a larger waist size. There is no fundamental limit in this process. Finally, the control of the guided atomic flux for a given and tunable narrow class of velocities as studied here is reminiscent of the quantum modulated transistor principle where the gate voltage is replaced by the modulation [35].

We acknowledge financial support from the Agence Nationale pour la Recherche, the Région Midi-Pyrénées, the university Paul Sabatier (OMASYC project), the NEXT project ENCOQUAM and the Institut Universitaire de France.

[1] B. G. Klappauf, W. H. Oskay, D. A. Steck, and M. G. Raizen, *Phys. Rev. Lett.* **81**, 1203 (1998).
[2] J. Ringot, P. Szriftgiser, J. C. Garreau, and D. Delande, *Phys. Rev. Lett.* **85**, 2741 (2000).
[3] W. K. Hensinger *et al.*, *Nature* **412**, 52 (2001).

[4] D. A. Steck, W. H. Oskay and M. G. Raizen, *Science* **293**, 274 (2001).
[5] J. Chabé, G. Lemarié, B. Grémaud, D. Delande, P. Szriftgiser, and J. C. Garreau, *Phys. Rev. Lett.* **101**, 255702 (2008).

- [6] H. Lignier, C. Sias, D. Ciampini, Y. Singh, A. Zenesini, O. Morsch, and E. Arimondo, *Phys. Rev. Lett.* **99**, 220403 (2007).
- [7] E. Kierig, U. Schnorrberger, A. Schietinger, J. Tomkovic, and M. K. Oberthaler, *Phys. Rev. Lett.* **100**, 190405 (2008).
- [8] Y.-A. Chen, S. Nascimbène, M. Aidelsburger, M. Atala, S. Trotzky, and I. Bloch, *Phys. Rev. Lett.* **107**, 210405 (2011).
- [9] R. Jördens, N. Strohmaier, K. Günter, H. Moritz and T. Esslinger, *Nature* **455**, 204 (2008).
- [10] S. D. Huber, B. Theiler, E. Altman, and G. Blatter, *Phys. Rev. Lett.* **100**, 050404 (2008).
- [11] M. Henseler, T. Dittrich, and K. Richter, *Phys. Rev. E* **64**, 046218 (2001).
- [12] A. Alberti, G. Ferrari, V. V. Ivanov, M. L. Chiofalo and G. M. Tino, *New J. Phys.* **12**, 065037 (2010) .
- [13] S. Arlinghaus and M. Holthaus, *Phys. Rev. A* **84**, 063617 (2011).
- [14] C. E. Creffield and F. Sols, *Phys. Rev. A* **84**, 023630 (2011).
- [15] M. Büttiker and R. Landauer, *Phys. Rev. Lett.* **49**, 1739 (1982).
- [16] R. H. Blick, D. W. van der Weide, R. J. Haug, and K. Eberl, *Phys. Rev. Lett.* **81**, 689 (1998).
- [17] G. Platero and R. Aguado, *Phys. Rep.* **395**, 1 (2004).
- [18] C. M. Fabre, P. Cheiney, G. L. Gattobigio, F. Vermersch, S. Faure, R. Mathevet, T. Lahaye, and D. Guéry-Odelin, *Phys. Rev. Lett.* **107**, 230401 (2011).
- [19] A. Couvert, M. Jeppesen, T. Kawalec, G. Reinaudi, R. Mathevet and D. Guéry-Odelin, *Europhys. Lett.* **83**, 50001 (2008).
- [20] G. L. Gattobigio, A. Couvert, M. Jeppesen, R. Mathevet, and D. Guéry-Odelin, *Phys. Rev. A* **80**, 041605 (2009).
- [21] Yu. B. Ovchinnikov, J. H. Müller, M. R. Doery, E. J. D. Vredenburg, K. Helmerson, S. L. Rolston, and W. D. Phillips, *Phys. Rev. Lett.* **83**, 284 (1999).
- [22] If a denotes the acceleration experienced by the atoms during the magnetic pulse, one finds $K = at_{\text{acc}}(t_{\text{acc}}/2 - t_{\text{prog}})$.
- [23] See the supplementary material (EPAPS document XXXX) for more details.
- [24] N. W. Ashcroft and N. D. Mermin, *Solid State Physics* (W. B. Saunders Co., Philadelphia, 1976).
- [25] Jon H. Shirley, *Phys. Rev.* **138**, B979 (1965).
- [26] This assumption suffices to capture all observed phenomena on the experiment. The extension to larger Floquet excitations is straightforward.
- [27] One can show indeed that the quasi energy of the propagating state of the incident particle inside the lattice is equal to its incident energy.
- [28] K. Drese and M. Holthaus, *Eur. Phys. J. D* **5**, 119 (1999).
- [29] L. D. Landau and E. M. Lifshitz, *Quantum mechanics: Non-relativistic theory*, 3rd ed. (Pergamon, New York, 1977), pp. 342-351.
- [30] C. Zener, *Proc. R. Soc. London Ser. A* **137**, 696 (1932).
- [31] The asymptotic values that enter Eq. (5) are obtained by a quadratic approximation of the energy difference $|\varepsilon_n - \varepsilon_{n\pm 1}|$. This ensures the robustness of the calculation of the Landau Zener probability.
- [32] S.-I. Chu and D. A. Telnov, *Physics Reports* **390**, 1 (2004).
- [33] The simple picture of two independent frequencies breaks down when the frequency difference is below 0.5 kHz.
- [34] C. Cohen-Tannoudji and D. Guéry-Odelin, *Advances in atomic physics: an overview* (World Scientific, Singapore, 2011).
- [35] F. Sols, M. Macucci, U. Ravaioli and K. Hess, *J. Appl. Phys.* **66**, 3892 (1989).